TEMPERING EFFECTS IN STEEL PARTS PRODUCED BY ADDITIVE FABRICATION USING LASER POWDER DEPOSITION

L. Costa[1], R. Colaço[1], T. Réti[2], A. M. Deus[1], R. Vilar[1]

[1] Instituto Superior Técnico, DEMat, Av. Rovisco Pais, 1049-001 Lisboa, Portugal
linocosta@ist.utl.pt
[2] Szechenyi Istvan University, Egyetem ter 1., H- 9026 Györ, Hungary

Abstract

Laser processed tool steels present a metastable structure generally containing martensite and an extremely large proportion of retained austenite as compared to conventionally treated steel, which affects considerably the properties of the material. In rapid tooling by laser powder deposition, as consecutive layers of material are deposited to generate a 3D object, the material in previously deposited layers is submitted to successive thermal cycles, which destabilise retained austenite, leading to its transformation to martensite. Also, the martensite present in these layers will progressively decompose by tempering when the material is reheated. As a result, the properties of the material are progressively modified as the object is built-up. The evolution of the microstructure and properties of tool steels during laser freeform manufacturing is extremely difficult to study experimentally, due to the complexity of the transformations involved and the heterogeneity of the material and of the applied thermal field, hence modelling presents clear advantages in the optimization of part build-up strategy. In the present work, a model of the phase transformations resulting from the successive overlap of clad layers based on the coupling of finite element calculations of the time-dependent temperature distribution with transformation kinetics is described. The model was used to predict the evolution of properties and final property distribution in a martensitic stainless steel component produced by laser powder deposition.

Keywords

Laser, Modelling, Phase Transformations, Rapid Manufacturing, Steel.

Introduction

Laser powder deposition (LPD) [1-4] is a rapid manufacturing technique that allows fully dense near-net-shape metallic components to be directly produced from a CAD file. In this process a material in powder form is injected in a high power laser beam and melted simultaneously with a thin layer of the substrate to form a continuous material track. Scanning the laser beam under numerical control (NC) and partially overlapping individual tracks in a suitable pattern produces continuous layers of material. By overlapping such layers defect-free three dimensional objects can be generated. In order to model the evolution of the properties of materials deposited by LPD [5, 6], the microstructure formed during solidification and the phase transformations that occur during the deposition process must be known. Previous work on laser surface melting (LSM) of tool steels [7-13] provide an adequate basis for studying the phenomena involved and predicting the microstructure and properties of steel tools produced by LPD. Colaço et al. carried out a detailed study of microstructure formation in laser surface melting of the martensitic stainless steel AISI 420 [7] and identified the influence of the laser processing parameters on the final microstructure [8]. The solidification microstructure in the laser processed material consists essentially of austenite dendrites and a very small proportion of interdendritic carbides. Austenite partially transforms to martensite during cooling. The volume fraction of retained austenite in the laser treated steel increases with decreasing laser power density and increasing scanning speed, and may reach almost 100 %. This large proportion of retained austenite is explained because, on one hand, in constrained solidification, the austenitic primary solidification mode is kinetically favoured as compared to the equilibrium ferritic primary solidification mode [7]. On the other hand, since the amount of carbides formed during solidification is negligible [9,10], austenite should be largely supersaturated in alloying elements. This, together with the small dendrite size in the laser treated material stabilizes austenite and inhibits its transformation to martensite [8].

These results show that the microstructure and properties of isolated tracks of tool steels produced by LPD depend essentially of the processing parameters used, but during multilayer deposition, tempering of the previously deposited material may

occur during the successive anisothermal cycles resulting from consecutive layer overlap. Tempering of laser treated tool steels at low temperatures does not change significantly the microstructure of the laser treated steel, but when the temperature exceeds 575 ºC retained austenite is destabilized and transforms into lath type martensite during subsequent cooling [9]. Destabilization of austenite is due to the precipitation of M_7C_3 type carbides within austenite. The release of internal stresses and partial recovery of austenite and martensite may also play a role. A tempering hardness peak similar to the secondary hardening peak is observed, but the temperature of maximum hardness is higher than the secondary hardening temperature (600 ºC as compared to 500 ºC). The hardening mechanisms are different from those occurring in conventional tempering as well, because the major contribution to the materials strengthening is the formation of martensite. These results show that, considerable changes in the microstructure and properties of the material should be expected due to solid-state transformations caused by layer overlap reheating. In fact, depending on the maximum temperature attained during each cycle, several precipitation reactions may be activated within both austenite and martensite, which will modify the microstructure and properties of the material. Precipitation reactions within austenite will also lead to the destabilization of this phase allowing its partial or total transformation to martensite. This new martensite will also be tempered by subsequent thermal cycles. Besides, if the temperature rises into the critical temperature range, partial or total austenitization may occur. Tempering of martensite, precipitation within retained austenite, austenitization and transformation of austenite into martensite may all occur. The influence of this complex set of transformations on the microstructure and properties of the material is extremely difficult to analyse experimentally and mathematical modelling must be used to optimize the part build-up strategy. The current paper describes a three-dimensional thermo-kinetic model of the LPD process, which combines phase transformation kinetics with finite element heat transfer calculations in order to calculate the evolution of the material microstructure and properties during laser freeform manufacturing. The deposition of an 8 layer wall of AISI 420 steel (0.33 %C, 0.4 %Mn, 0.5 %Si, 13.5 %Cr) on a large substrate of the same material was used as a case study.

Thermo-kinetic model

The model used to perform simulation of LPD consists of a 3D finite element heat transfer module coupled with a phase transformations routine. The temperature field calculated by the heat transfer module is used to determine the ongoing phase transformations, according to the sequence described in the flow chart of figure 1. It is assumed that solidification starts with the formation of austenite dendrites and that, upon cooling, this austenite can only transform into martensite. However, martensite laths do not cross dendritic boundaries and therefore stabilization of austenite due to grain size refinement must be considered. This requires knowledge of the grain size of the microstructure formed during solidification, estimated from calculations of the primary dendrite spacing using solidification theory. Semi-empirical solid-state phase transformation models determine the volume fractions of martensite and austenite and calculate the hardness of the material. The details of these models are discussed below.

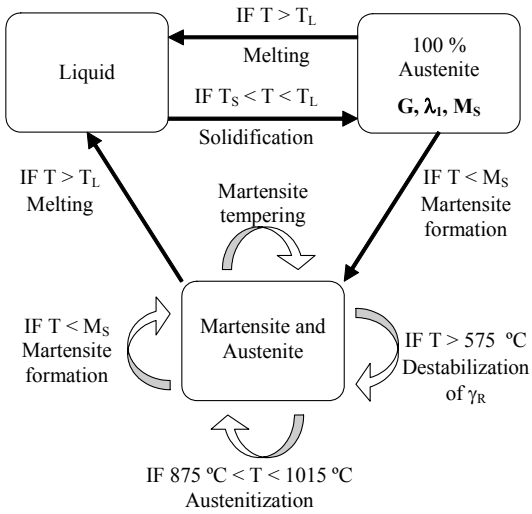

Figure 1 – Phase transformation sequence used to model the laser powder deposition process of AISI 420.

Solidification

As previously referred, it is assumed in the model that solidification starts with the formation of austenite dendrites [7]. Their primary dendrite spacing, λ_1, is estimated using the Kurz and Fisher [14] dendrite packing model:

$$\lambda_1 = \sqrt{\frac{3 \cdot (T_T - T_S) \cdot r}{G}}, \qquad (1)$$

where G is the mean temperature gradient at the solid – liquid interface (figure 2) and T_S is the solidus temperature of the material. The dendrite tip temperature and radius (T_T and r, respectively) are calculated as a function of the solidification speed, V_S, and temperature gradient, G, using the Kurz, Giovanola and Trivedi [15] model for the directional

growth of dendrites, as modified by Rappaz et al. [16] for ternary alloys:

$$\frac{4\cdot\pi\cdot\Gamma}{r^2}+\frac{1}{r}\cdot\sum_{i=1}^{2}\frac{2\cdot Pe_i\cdot C_{o,i}\cdot m_i\cdot(1-K_i)}{\left[1-(1-K_i)\cdot Iv(Pe_i)\right]}+G=0\,,$$

$$Pe_i=\frac{r\cdot V_s}{2\cdot D_i}\,, \qquad (2)$$

$$T_T=T_L+\Delta T_T\,, \qquad (3)$$

$$\Delta T_T=\sum_{i=1}^{2}\frac{m_i\cdot C_{o,i}}{\left[1-(1-K_i)\cdot Iv(Pe_i)\right]}-\sum_{i=1}^{2}m_i\cdot C_{o,i}-\frac{2\cdot\Gamma}{r},$$

where $Iv(Pe_i)=Pe_i\cdot\exp(Pe_i)\cdot\int_{Pe_i}^{\infty}\frac{\exp(-z)}{z}dz$ is the Ivantsov function and Pe_i the Peclet number for solute component i. The solidification speed, V_S, is related to the laser scanning speed, V_L, by $V_S = V_L \cdot \cos\theta$ (figure 2), where θ is the angle between the laser scanning speed vector and the normal to the solid-liquid interface [16]. The values of the thermodynamic properties of AISI 420 tool steel used in the calculation are presented in Table 1 [7].

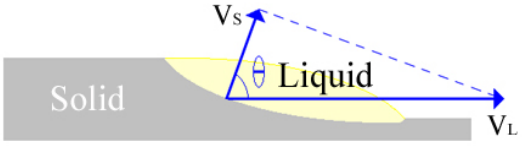

Figure 2 – Detail of the melt pool during laser powder deposition.

Martensitic transformation

On the assumption that the deposition is performed on a large substrate, which acts as an effective heat sink, the cooling rates generated in LPD are high enough to suppress diffusional solid-state phase transformations. Therefore, the austenite formed during solidification can only transform into martensite. Austenite will transform to martensite as soon as the temperature drops below the martensite start temperature, Ms. In the present model, the Ms temperature is calculated on the basis of the chemical composition of the steel, using Andrews equation [17] (equation 4a). However, as martensite laths do not cross dendritic boundaries [8], stabilization of austenite due to grain size refinement must be considered. This effect can be incorporated if the value of Ms is calculated as a function of the microstructure grain size, d, (equation 4b), as proposed by Jiang et al. [18].

$$Ms_{ANDREWS} = 512 - 453\cdot(\%C) - 15\cdot(\%Cr) \qquad (4a)$$

$$Ms_{ANDREWS} = 160\ ºC.$$

$$Ms\,(d) = Ms_{ANDREWS}\cdot\exp(-B/d)\quad (ºC). \qquad (4b)$$

The volume fraction of martensite f_α is calculated using Koistinen and Marburger equation [19] (equation 5),

$$f_\alpha = 1 - f_{\gamma_0}\cdot\Phi(T),$$
$$\Phi(T)=\begin{cases}1 & ,if\ \ T\geq Ms\\ e^{(-0.011\cdot(Ms-T))} & ,if\ \ T<Ms\end{cases}, \qquad (5)$$

where $f_{\gamma 0}$ is the initial volume fraction of austenite. In the present model, d is replaced by the primary dendrite spacing, λ_1, and it is assumed that B≈1 for d in μm.

Martensite tempering

It is assumed in the model that the change in hardness of martensite during tempering under anisothermal conditions can be quantified using equation 6, as proposed by Réti et al. [20]. H_0 is the initial hardness of the as-quenched martensite, Q the activation energy and R the universal gas constant. A and m are fitting constants. Tempering of alloy steels activates several competing precipitation reactions [21], amongst which are those responsible for secondary hardening. Since several reactions may occur simultaneously, the activation energy was replaced by an effective activation energy, defined as proposed by Mittemeijer [22] as the weighted linear combination of the activation energies of the individual precipitation reactions that occur during tempering. For AISI 420 steel the values of these parameters were estimated on the basis of conventional quenching and isothermal tempering experiments performed by the authors, leading to the effective activation energy presented in figure 3 and to H_0 = 658 HV, A = 1300 HV/s and m = 0.055. Based on this experimental information, the corresponding 1 hour isothermal tempering curve was calculated using equation 6 (figure 3).

$$H(P_D) = H_0 - A\cdot(P_D)^m =$$
$$H(P_D) = H_0 - A\cdot\left[\int_0^{t_F} e^{-Q/(R\times T)}\cdot dt\right]^m. \qquad (6)$$

Tempering above 575 ºC destabilizes retained austenite, γ_R, [9] and this phase will transform, at least partially, to martensite during subsequent cooling, when the temperature drops below the Ms

temperature. Austenitizing occurs when the temperature reaches the austenitic transformation range. For AISI 420 steel Ac_1 and Ac_3 temperatures are respectively equal to 875 and 1015 ºC (considering a heating rate of 2400 ºC/s) [23] and it was assumed that the volume fraction of austenite increases linearly with temperature between these temperatures.

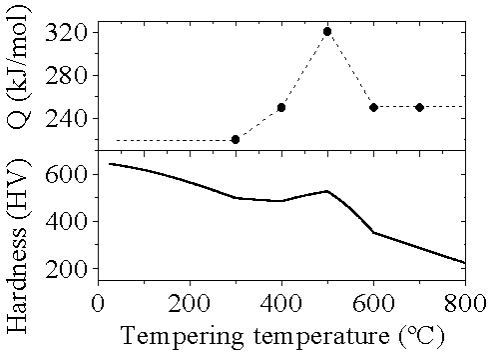

Figure 3 – Activation energy and corresponding 1 hour tempering curve, calculated using equation 6, for AISI 420 tool steel.

Implementation

The finite element calculations were performed sequentially, as a series of constant geometry problems (named steps), linked together by introducing the output of problem **n** as the initial conditions for problem **n+1** [6]. The progressive change of the object shape was modelled by adding a finite number of cubic solid elements at the beginning of each step. A heat flux boundary condition, modelling the irradiation of the surface elements by a focused Gaussian laser beam, was used to generate an adequately sized melt pool. Additional boundary conditions taking into consideration heat loss due to convection and thermal radiation and a zero heat flux along the symmetry plane of the problem were also applied. Figures 4 and 5 illustrate the geometry used. In each step, the average thermal conductivity and specific heat (Table 2) were calculated for each element as a function of the properties of individual phases, weighed by the respective volume fractions.

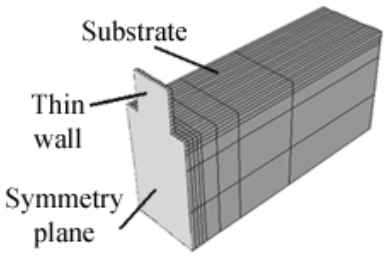

Figure 4 - General overview of the geometry.

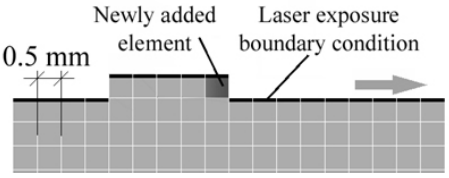

Figure 5 – Detailed 2D view of the symmetry plane, during deposition of the first layer.
Each layer of material is built by the addition of a row of 10 elements, each with 0.5^3 mm^3.

This 3D thermo-kinetic finite element model was used to simulate multilayer LPD of a thin wall of AISI 420 tool steel, using a 1300 W Gaussian laser beam focused into a 3.0 mm diameter spot (measured at e^{-2} of maximum intensity), moving at 20 mm/s and with a powder feed rate of 0.1 g/s and powder use efficiency of 78%. A laser power absorption coefficient of 25% was considered. For 1.0 mm wide tracks, these conditions require the addition of 1×1×2 cubic elements (each occupying a volume of 0.5^3 mm^3) during each material addition step (25 ms long). A total of eight layers of material, each 5.0 mm long and 0.5 mm thick, were overlapped on a substrate of the same material in the pre-treated condition (quenched and tempered at the secondary hardening temperature). The initial temperature of the added material was 1450 ºC. Each new layer was initiated with the laser beam positioned at X_i (figure 6) during a step of 75 ms, to create a melt pool before the addition of material. During the subsequent material deposition steps, the laser beam was moved continuously 0.5 mm ahead of the newly deposited elements, up to the position X_f (figure 6), where it was switched off. A delay of 10 seconds between consecutive tracks allowed the material to cool down before the addition of a new layer. After the deposition of the 8th layer, a final cooling step of 60 seconds allowed the part to cool down to a temperature close to room temperature. An average solidification speed, V_S, of 10 mm/s was assumed (from an average $\theta = 60º$ in figure 2). The mean temperature gradient G used in equation 1 was evaluated as the temperature gradient at the time instant when the solidification condition is satisfied ($T_S < T < T_L$). However, since the temperature gradient does not significantly affect the dendrite tip radius or tip temperature [16], a constant temperature gradient of 10^6 K/m was used for the Kurz, Giovanola and Trivedi model calculations, yielding r = 0.65 μm, and ΔT_T = - 4.5 ºC.

Results

The results obtained are presented in figures 6 to 11. The information provided concerns the symmetry plane of the part. The temperature distributions at the end of the deposition of the 2nd

(figure 6) and 8th (figure 7) layers (before the 10 second cooling step) clearly show that the depth of the heat affected zone (HAZ) increases with increasing wall height. The proximity of the base material, which acts as a heat sink, promotes higher cooling rates in the first case (figure 6), as shown by a shorter distance between isotherms (higher temperature gradient), than in the second case (figure 7), where the cooling rate is limited by heat conduction along the thin wall. It is clear that the processing parameters used in the calculations produce an adequately sized melt pool, with limited fusion of the previous layer. However, the length of the melt pool increases with increasing height of the wall, certainly due to the lower cooling rates.

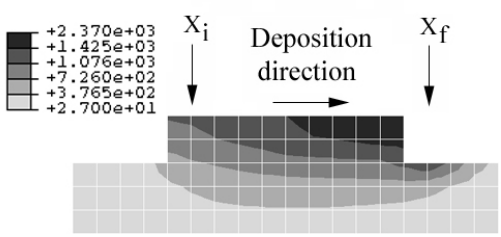

Figure 6 – Temperature field (ºC) at the end of the last deposition step of the 2nd layer.

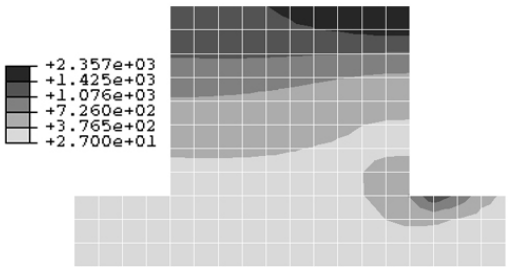

Figure 7 – Temperature field (ºC) at the end of the last deposition step of the 8th layer.

This variation in the cooling conditions along the wall height is also visible in figure 8. The temperature gradient at the solid - liquid interface decreases almost an order of magnitude from the first to the last layers, thus changing the primary dendrite spacing distribution (figure 9), as predicted by the Kurz and Fisher model (equation 1). After solidification, the austenite in the first layer presents an average λ_1 of 10.0 μm. As the material quenches down to room temperature, about 70 % of the austenite transforms into martensite (according to equations 4 and 5). However, as successive layers of material are overlapped, retained austenite progressively destabilizes and transforms into martensite, as shown in the final map of transformed austenite (figure 10), obtained after the final 60 s cooling step when the average part temperature has dropped to 68 ºC. The proportion of martensite attains nearly 100 % in the first 4 layers and progressively decreases down to about 60 % in the last 2 layers. As seen in figure 7, the heat input due to the deposition of the 8th layer completely austenitizes the previous one.

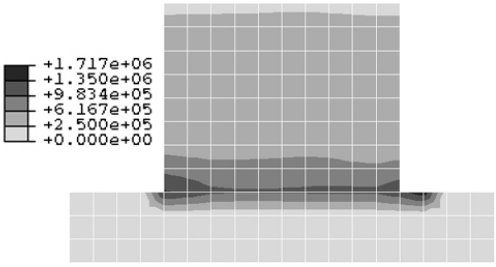

Figure 8 – Temperature gradient (ºC/m) at the solid – liquid interface.

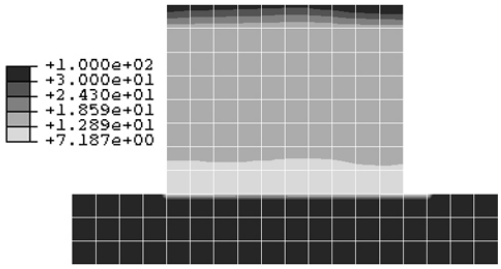

Figure 9 – Primary dendrite spacing λ_1 (μm).

Besides destabilizing retained austenite, the successive anisothermal thermal cycles due to layer overlapping also lead to martensite tempering, thus reducing the material hardness, as shown in figure 11. It is interesting to note that the calculations predict a maximum hardness (above 500 HV) in the top layer of the wall, despite the presence of a large proportion of retained austenite. This is due to the existence of 60 % of fresh martensite, which is much harder than the tempered martensite found in the lower layers.

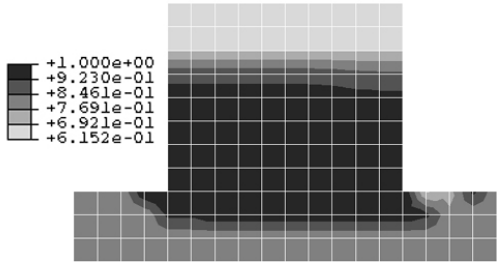

Figure 10 – Final distribution of transformed austenite.

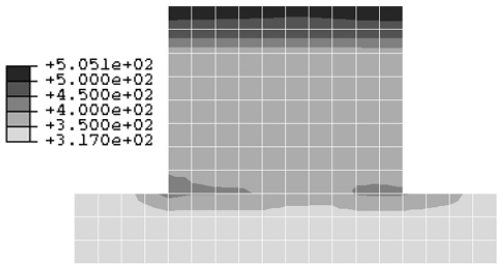

Figure 11 – Final hardness map (HV).

Conclusions

A 3D thermo-kinetic finite element model of the laser powder deposition process was developed to simulate microstructure evolution during laser freeform manufacturing. The model was applied to the deposition of an 8 layer wall of AISI 420 tool steel and the final microstructure and properties of the material determined. The results show that there is a significant change in the heat conduction conditions as the wall height increases, leading to an increase of the melt pool length and depth of the heat affected zone and a decrease of the temperature gradient at the solid - liquid interface. This latter feature leads to an increase of the microstructure scale along the wall height, thus increasingly facilitating the austenite-to-martensite transformation upon cooling. As successive layers are overlapped retained austenite is destabilized and martensite softens by tempering, leading to a progressive change of the microstructure and properties of the material, as the wall is being built. At the end of the deposition process, the first layers are composed essentially of tempered martensite with hardness between 350 and 400 HV while the top layers contain a mixture of fresh martensite and 40 % retained austenite, with an average hardness of 500 HV.

Annex

Table 1 – Thermodynamic data used to calculate the dendrite tip radius and temperature [7].

		C	**Cr**
Slope of the liquidus surface due to component i	m_i	-70 K wt% $^{-1}$	-2.1 K wt% $^{-1}$
Equilibrium partition coefficient of component i	K_i	0.50	0.92
Concentration of component i in the alloy (%)	$C_{o,i}$	0.33	13.5
Diffusion coefficient of component i	D_i	1.8×10^{-8} m^2 s^{-1}	2×10^{-9} m^2 s^{-1}
Gibbs-Thomson coefficient	Γ	1.9×10^{-7} Km	
Liquidus temperature of AISI 420	T_L	1425 ºC	
Solidus temperature AISI 420	T_S	1375 ºC	

Table 2 - Material properties used in the finite element model [24, 25].

Temperature (ºC)	-	27	300	600	800	900	1100	1300	1410	1425
Thermal Conductivity (W/m·K)	α	43.1	36.7	30.1	-	-	-	-	-	-
	γ	15.0	18.0	21.7	25.1	26.8	28.9	32.8	-	34.0
Specific Heat (J/kg·K)	α	485	574	654	-	-	-	-	-	-
	γ	535	568	603	632	-	-	760	750	-
Density (kg/m^3)	-	7750	-	-	-	-	-	-	-	-
Latent heat of fusion (kJ/kg)	-	-	-	-	-	-	-	-	-	250
Hardness (HV)	Fresh martensite			658						
	Austenite - γ			280						

Acknowledgements

L. Costa gratefully acknowledges financial support from Fundação para a Ciência e Tecnologia. The authors also acknowledge GRICES for the financial support (project: Repairing of machine parts by laser cladding – Proc. 4.1.1 OMFB).

References

[1] R. Vilar; Int. J. Powder Metall., 2001, Vol. 37, 2, 31-48.

[2] J. W. Sears; Int. J. Powder Metall., 2001, Vol. 37, 2, 29-30.

[3] J. Mazumder; A. Schifferer; J. Choi; Mater. Res. Innov., 1999, Vol. 3, 3, 118-131.

[4] O. Graydon; Opto & Laser Europe, 1998, Vol. 47, 33-35.

[5] L. Costa; T. Reti; A. M. Deus; R. Vilar; 2002 International Conference on Metal Powder Deposition for Rapid Manufacturing, D. Keicher; J. W. Sears; J. E. Smugeresky, Eds.; MPIF, San Antonio, Texas, USA, 2002, 172-179.

[6] L. Costa; A. M. Deus; T. Reti; R. Vilar; RPD 2002 - Advanced solutions and development; CENTIMFE, Marinha Grande, Portugal, 2002.

[7] R. Colaço; R. Vilar; Surf. Eng., 1996, Vol. 12, 4, 319-325.

[8] R. Colaço; R. Vilar; J. Mater. Sci. Lett., 1998, Vol. 17, 563-567.

[9] R. Colaço; R. Vilar; Scr. Mater., 1998, Vol. 38, 1, 107-113.

[10] R. Vilar; R. Colaço; D. Colin; O. Conde; 3rd European Conference on laser treatment of materials - ECLAT'90, H. W. Bergmann; R. Kupfer, Eds.; Sprechsaal Publishing Group, Erlangen, Germany, 1990, Vol. 1, 377-388.

[11] J. C. Ion; T. Moisio; T. F. Pedersen; B. Sorensen; C. M. Hansson; J. Mater. Sci., 1991, Vol. 26, 43-48.

[12] J. M. Belló; V. López; B. J. Fernández; J. Ruiz; P. Sanz; F. Zubiri; Rev. Metal. Madrid, 1991, Vol. 27, 3, 147-162.
[13] P. A. Molian; W. E. Wood; Mater. Sci. Eng. 1984, Vol. 62, 271-277.
[14] W. Kurz; D. J. Fisher, Fundamentals of Solidification, Trans Tech Publications Ltd, 1998.
[15] W. Kurz; B. Giovanola; R. Trivedi; Acta Metall., 1986, Vol. 34, 5, 823-830.
[16] M. Rappaz; S. A. David; J. M. Vitek; L. A. Boatner; Metall. Trans. A, 1990, Vol. 21, 1767-1782.
[17] K. W. Andrews; J. Iron Steel Int., 1965, Vol. 203, 721-727.
[18] B. H. Jiang; L. Sun; R. Li; T. Y. Hsu; Scr. Metall. Mater., 1995, Vol. 33, 1, 63-68.
[19] D. P. Koistinen; R. E. Marburger; Acta Metall., 1959, Vol. 7, 59-60.
[20] T. Réti; M. Gergely; P. Tardy; Mater. Sci. Technol., 1987, Vol. 3, 365-371.
[21] R. W. K. Honeycombe; H. K. D. H. Bhadeshia; Steels - Microstructure and properties, Edward Arnold, 1995.
[22] E. J. Mittemeijer; J. Mater. Sci., 1992, Vol. 27, 3977-3987.
[23] A. Rose; W. Peter; W. Strassburg; L. Rademacher, Atlas zur Warmebehandlung der stahle, Veralg Stahleisen M. B. H., 1961.
[24] H. K. D. H. Bhadeshia in Handbook of residual stress and deformation of steel, G. Totten; M. Howes; T. Inoue, Eds.; ASM International, 2002.
[25] G. D. Morwood; Thesis, The University of Queensland, 2000.

Biography

Lino Costa has a degree in Physics Engineering and is a Ph.D. candidate at Instituto Superior Técnico, Lisbon, Portugal.

Rogério Colaço has a PhD in Materials Engineering and is a professor at the Department of Materials Engineering of Instituto Superior Técnico, Lisbon, Portugal.

Augusto Moita de Deus is an Assistant Lecturer at the Department of Materials Engineering of Instituto Superior Técnico, Lisbon, Portugal and a Ph.D. candidate at the University of Illinois at Urbana-Champaign, USA.

Tamás Reti is a professor of applied computer science at the Szechenyi Istvan University, Egyetem ter 1., H- 9026 Györ, (Hungary), where he specializes in modeling of transformation phenomena in alloys. He is the author of over 70 scientific paper. He is the co-chairman of the ASM Technical Committe on Modeling of Heat Treatment Processes.

Rui Vilar is an associate professor at the Department of Materials Science and Engineering of Instituto Superior Técnico, at Lisbon, Portugal. He is the leader of the Laser Materials Processing Group at Instituto Superior Técnico and his research interests are laser materials processing and surface engineering. He is a member of LIA, SPIE, MRS, TMS, ASM, AWS, and The Institute of Materials (U.K.)